Study of variability in dynamic simulations of turnouts using the PGD method

Demeng Fan, Michel Sebès, Aquib Qazi, C Pozzolini, Emmanuel Bourgeois

Taylor & Francis
Taylor & Francis Group

Vehicle System Dynamics

International Journal of Vehicle Mechanics and Mobility

ISSN: (Print) (Online) Journal homepage: https://www.tandfonline.com/loi/nvsd20

Study of variability in dynamic simulations of turnouts using the PGD method

D. Fan, M. Sebès, A. Qazi, C. Pozzolini & E. Bourgeois

To cite this article: D. Fan, M. Sebès, A. Qazi, C. Pozzolini & E. Bourgeois (2023) Study of variability in dynamic simulations of turnouts using the PGD method, Vehicle System Dynamics, 61:3, 905-922, DOI: 10.1080/00423114.2021.1977832

To link to this article: https://doi.org/10.1080/00423114.2021.1977832

Published online: 20 Sep 2021.

VEHICLE SYSTEM DYNAMICS
2023, VOL. 61, NO. 3, 905–922
https://doi.org/10.1080/00423114.2021.1977832

IAVSD
Taylor & Francis
Taylor & Francis Group

REVIEW ARTICLE

OPEN ACCESS Check for updates

Study of variability in dynamic simulations of turnouts using the PGD method

D. Fan [a,b], M. Sebès[a], A. Qazi [a,b,c], C. Pozzolini[b] and E. Bourgeois[a]

[a]COSYS-GRETTIA, Univ Gustave Eiffel, Marne-la-Vallée, France; [b]ESI Group, Paris, France; [c]Laboratoire Navier, Ecole des Ponts ParisTech, Univ Gustave Eiffel, CNRS, Marne-la-Vallée, France

ABSTRACT

The design and maintenance of turnouts implies considering a great number of external factors that have an effect on their structural integrity. The proper generalised decomposition (PGD) method is used in this paper to carry out a parametrised study of the vehicle-track interaction in a non-intrusive way. The reduced model is built using a defined domain for some of the influence parameters: the vehicle speed, the wheel/rail friction coefficient and the axle load. A major assumption of the PGD solution is its ability to express quantities of interest in a separated form. One of the goals is to show the relevance of separability in the field of railway dynamics. The example of a switch is chosen as a validation of method. The output of the PGD model is the dissipated energy per metre in the switch rail. The robustness of the reduced model is verified using the complete solution. Probabilistic simulations are carried out in order to explore the possibility of using the PGD solution as a numerical abacus in dynamic simulations of switches and crossings. These first tests show that the PGD solution is a promising reduction model method in railway dynamics.

ARTICLE HISTORY
Received 19 January 2021
Revised 27 July 2021
Accepted 2 September 2021

KEYWORDS
Switch & crossing; railway dynamics; wheel/rail contact; model order reduction; proper generalised decomposition; data-driven technique; Monte Carlo

1. Introduction

Vehicle-track interaction is a major cause of damage for the different mechanical installations used in the railway network. The maintenance and replacement of the railway network devices necessitate significant economic and labour costs. Even among the different railway devices, the turnout presents quite a special case for which the vehicle-track interaction is more difficult to handle than in the case of a normal rail, since it depends on complex factors such as the varying section, the multi-contact, and the deformation of several rail bodies. The design, maintenance and the exploitation of turnouts implies addressing these issues, as well as considering a great number of other external factors that have an effect on their structural integrity such as:

- the class of rolling stocks: locomotive, electrical multiple unit (EMU) or freight wagons, to name a few,

CONTACT D. Fan demeng.fan@univ-eiffel.fr

- the wheel profiles: different classes of nominal profiles, and worn profiles with various patterns and levels of wear,
- the track settlement: ballasted tracks or slab track systems; and their changing structural properties,
- wheel/rail adhesion: the friction coefficient, wet or dry conditions, brake or traction inducing high slip values,
- vehicle speed,
- axle load,
- initial conditions before entering the turnout,
- track geometry quality in terms of alignment and longitudinal levels,
- wear of rail profiles.

Although some studies have already considered this multivariate aspect through a design of experiments [1–3], the large number of factors affecting the rail damage inhibits the manufacturers of the railway devices and the operators of the railway networks from building an explicit rail damage prediction tool in the form of a numerical abacus. In a single dynamic simulation, the parameters affecting the rail damage are kept constant. For a given set of parameters, it is possible to assess the potential damage by using such criterion as the T_γ function [4], which represents the dissipated energy per metre. In the estimation of the rail damage, the wear, related to the T_γ function, is not the sole factor to consider. Other criteria, such as the maximal contact pressure, related to the rolling contact fatigue, also have an impact in the durability of the turnout. However, Pållson has shown in [5] that the maximal pressure and the T_γ function are highly correlated in a switch panel which allows, in a first approach, the choice of the T_γ as the only criterion in order to verify the feasibility of the method.

However, evaluating a response surface characterising the T_γ function for all values of the parameters requires performing huge sets of computations. Furthermore, these computations will result in a model too large to be exploited for subsequent tasks such as design optimisation, inverse analysis, or probabilistic studies in order to represent the uncertainty or variability of different input parameters.

Various methods of model order reduction have been proposed in order to handle multi-parametric problems, for instance, the proper orthogonal decomposition and the reduced basis method [6]. First works combining data-driven technologies and computational mechanics were achieved in the 2000s [7–10]. Bases are often obtained from a set of offline solutions. The reduced basis maintains an accurate enough solution with a certain loss of generality but enables impressive computing time savings. To improve the generality, an appealing way is to establish the reduced basis and solve the partial differential equation (PDE) based problem at the same time [6]. However, this latter option is extremely intrusive from a practical point of view, as the discretized PDEs have to be reformulated in the source code in order to consider design parameters. A lot of industrial problems, for instance in railway dynamics, are solved by dedicated software where the intrusive option may not be implemented easily. Some non-intrusive methods have been presented in the literature [11–13]. Moreover, the so-called sparse-proper generalised decomposition (s-PGD) method [13] has been shown to avoid overfitting and over-oscillating phenomena, and can be considered as a non-linear regression solver.

A space–time separated representation was first introduced by Ladevèze [14] in the context of the large time increment (LATIN) method, which can be seen as a precedent for the proper generalised decomposition (PGD) method developed in the context of multi-dimensional modelling of complex fluids, and subsequently applied in other domains [15]. The idea is to split the multi-dimensional problem into lower-dimensional problems defined not only in space and time, but also in other parameters such as the geometry, boundary conditions or material properties. The well–known curse of dimensionality is thus circumvented. The PGD solution is approximated as a truncated sum of modes and may subsequently be handled easily. The principle of separating representations has been recently extended to nonlinear regression applications in the s-PGD method [13].

The PGD method was used for the first time in [16, 17] in the field of railway dynamics in an intrusive way. To the knowledge of the authors, the present paper is a first application of the method in a non-intrusive way using the s-PGD method. This is an advantage as intrusiveness inevitably would require the modification of the source code [12], here the railway dynamics multi–body system (MBS) software. The main goal is to demonstrate its relevance in this context. The principle is to build a numerical abacus to be used 'online' that may handle some of the external parameters highlighted above for the specific case of a turnout. This abacus is created by first carrying out a finite number of 'offline' simulations using a design of experiments (DOE) approach. The principle of building a numerical abacus is not a novelty: in the fields of railway dynamics, the Kalker's book of tables USETAB [18] follows the same approach. The PGD method is still more versatile, as it allows to handle high dimensional domains. For instance, domains of up to ten dimensions may be handled [19] thanks to the separation of variables. Another difference is the model reduction, which allows to handle the model more easily for subsequent tasks, while keeping only the relevant information. A last difference lies in the nonlinearity of the PGD method. The same characteristics hold true for the s-PGD method. Here, railways dynamics simulations are handled with the MBS software VOCO [20], but other MBS packages may be used instead, as the process used in this paper does not require any modification in the source code of the MBS. The s-PGD method is then used to extract the expected behaviour of this complex multi-dimensional system. A parametric study of the damage in a switch rail is considered as a validation of the s-PGD method. The objective function is the T_γ function, used as a damage index in a switch, in an approach similar to the one in [5].

The paper is organised as follows. In section 2, the case studies are described with the chosen parameters. The objective function is defined and its s-PGD expression is given in order to build a response surface of the damage in the switch rail. The individual effects of the parameters on the objective function are qualitatively assessed, and the DOE is presented. In section 3, the procedure used to build the s-PGD solution is described. For the readers not familiar with the principle of the PGD method, an example of heat transfer equation solved by PGD in an intrusive way is given in the appendix. The robustness of the reduced model is studied in section 4. Probabilistic simulations are carried out with the reduced order model and the full approach, in order to demonstrate the relevance of the s-PGD solution. Finally, the conclusions are summarised in section 5.

2. Case study

2.1. Definition of the nominal case and range of variation of the parameters

A diagram of a turnout is illustrated in Figure 1. The switch panel is composed of a switch rail and a stock rail. The investigation of potential damage is limited in this paper to the area framed by the black dotted line. The structural integrity of a switch rail is investigated. The Swedish switch of the switches and crossings (S&C) benchmark [21] is considered. It is assumed that most of the damage is due to the diverging route and consequently only this configuration (run #4 of the S&C benchmark) is considered. The only modification in the settings concerns the vehicle, which is a Y25 freight wagon instead of the passenger coach used in the benchmark. The model of the vehicle is the freight Sgns (S: special flat wagon with bogies, g: max 60 feet containers, n: 60 tons max load, s: max speed 100 km/h) wagon built in the Dynotrain project: the axle loads vary between the empty configuration (5 tons) and the loaded one (25 tons) [22]. The same model in its loaded configuration has been used in a preceding study [23], showing satisfying results in comparison with experimental measurements [24]. The change of vehicle with respect to the S&C benchmark is motivated by the choice of the axle load as an input parameter in this first study, where the vehicle speed, the friction coefficient, and the axle load are chosen as the parameters of interest. The nominal values of these input parameters as used in the S&C benchmark for run #4 and their variations, are summarised in Table 1. The parametrisation of the wheel profile is not considered in the present case even though this parameter is known to play a significant role in the damage process [4, 5].

The dissipated energy per metre is approximated by the T_γ function [1]:

$$T_\gamma = \sum (F_x v_x + F_t v_t), \tag{1}$$

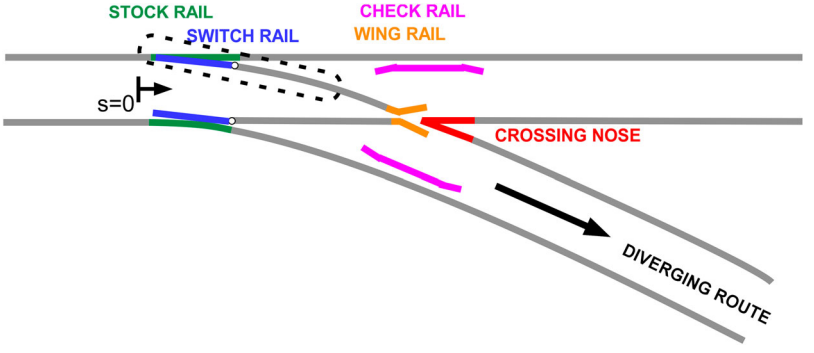

Figure 1. Turnout layout plan with diverging route in the facing traffic direction and rail body legends.

Table 1. Nominal values of parameters and their variations.

Variable	Description	Unit	Nominal Value	Min value	Max value	Step
v	Speed	km/h	80	10	100	10
q	Axle Load	ton	11.2	5	25.2	2.02
μ	Friction coefficient		0.35	0.07	0.7	0.07

where F_x and F_t are the tangent forces acting in the longitudinal and transverse directions respectively, while ν_x and ν_t are the creepages in the corresponding directions. This parameter is a function of the position x in the track. Only the outer wheel of the first wheelset is considered here, and the summation in the formula is on the number of contact patches at a given x, usually not exceeding two. To normalise the results, the objective function T_γ is divided by the axle load and the friction coefficient, which facilitates the building of the s-PGD solution.

2.2. An overview on the effects of different parameters

Figure 2 shows the evolution of the dissipated energy T_γ per metre of the switch rail for the S&C benchmark configuration, for the nominal values of this paper, and for various configurations where a single parameter is changed. The abscissa is the curvilinear track coordinate. Its origin is located at the front of the switch (Figure 1). The assumptions made for the MBS simulations in VOCO are detailed in [25]. Contact is established at about 4 m from the beginning of the turnout. This corresponds to a peak value located in the thinner part of the switch rail. The following observations can be made from the curves of Figure 2:

- Firstly, the result of the S&C benchmark may be compared with the nominal model of this paper. Settings are identical and the axle load is almost the same. The peak value remains almost unchanged, but more energy is dissipated with the freight wagon than with the passenger coach of the benchmark: this difference is due to the non-linearities of the suspension of the Y25 bogie. In the field of railway dynamics, it seems difficult to parametrise vehicles in the s-PGD solution. A damage function should be assigned to a given rolling stock, and the total damage be then summed according to the distribution of each vehicle passing the site [4].
- Secondly, the net effect of the friction coefficient and the axle load is visible through comparison with the nominal set of parameters (dotted curve). When the friction coefficient is raised to 0.42 instead of its nominal value 0.35, the energy dissipated in the switch rail is higher. A similar effect is observed when the axle load is raised from 11.2–15.9 tons
- Finally, the effect of the vehicle speed (40 versus 80 km/h in the nominal dotted curve) seems to be less significant.

2.3. Design of experiments

Input parameters are numerical values to be defined in a given range as shown in Table 1. Ten equally spaced values are considered for each parameter, with the vehicle speed between 10 and 100 km/h, the axle load between 5.0 and 25.2 tons, and the friction coefficient between 0.07 and 0.7. All the MBS simulations presented in this paper are carried out with a 2 CPU 3.6 GHz processor. A total of 1000 runs is carried out, which requires about two days calculation, in order to build the response surface of the T_γ function describing the effect of the three parameters. These 'off-line' simulations are carried out to construct the reduced s-PGD model. The T_γ function is a function of distance x from the front of

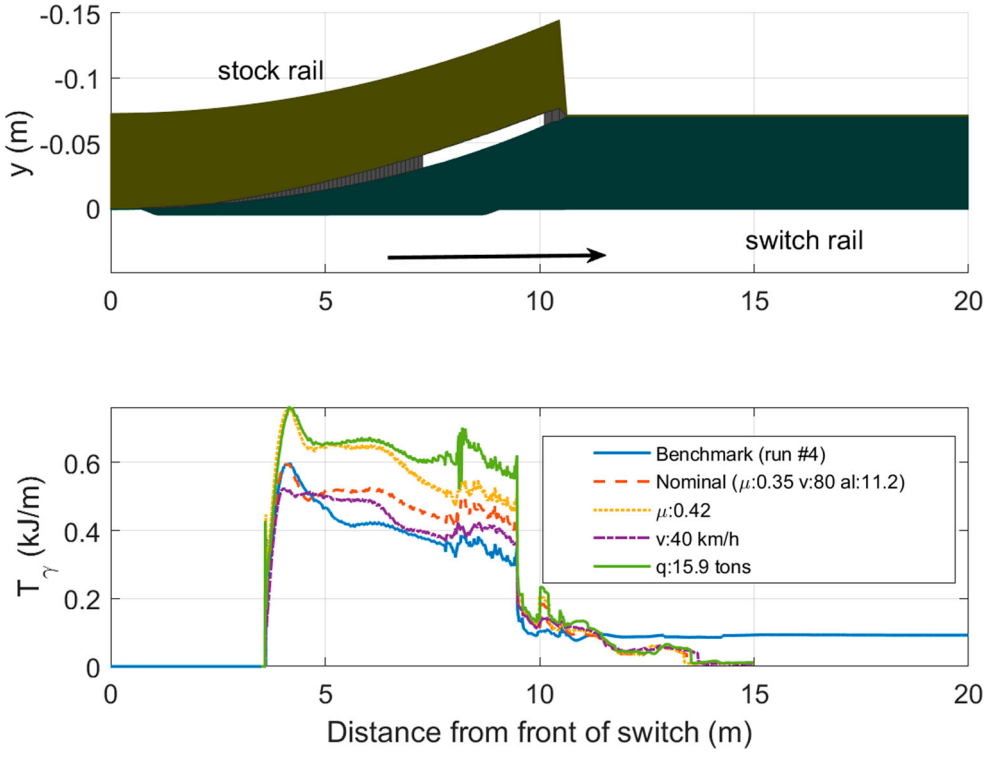

Figure 2. Influence of some input parameters on the Tγ in a switch rail.

the switch rail and three parameters. In the reduced model, the T_γ function is seen as the sum of products of functions of one of the three parameters v, q and μ for each x. In other words, the separated form of T_γ in the frame of s-PGD for a given x coordinate is expressed as:

$$T_\gamma{}^M(v, q, \mu, x) = \sum_{i=1}^{M} V_x^i(v) \cdot Q_x^i(q) \cdot U_x^i(\mu), \tag{2}$$

where the lower-case letters $v, qand\mu$ are respectively the speed, the axle load, the friction coefficient, while the upper-case letters V_x, Q_x and U_x are their respective functions at a given x. The index $i = 1, \ldots,$ M is the mode number. Normalising the objective function may ease the process of finding a robust s-PGD estimate. As tangent forces may not exceed Coulomb's limit, the input of the s-PGD builder is T_γ divided by the friction coefficient μ times the axle load q. In railway dynamics some variables usually have high-frequency contents: such is the case for the contact forces and the displacements of rail. If the objective function is one of these variables, numerical peaks of high frequency will cause problems for the building of the reduced solution and need to be filtered out. However, in the case of the T_γ, the phenomena of the high-frequency vibration is not severe. Additionally, filtering may introduce some negative values at the beginning of the switch rail while the T_γ is always positive. Consequently, the T_γ is not filtered.

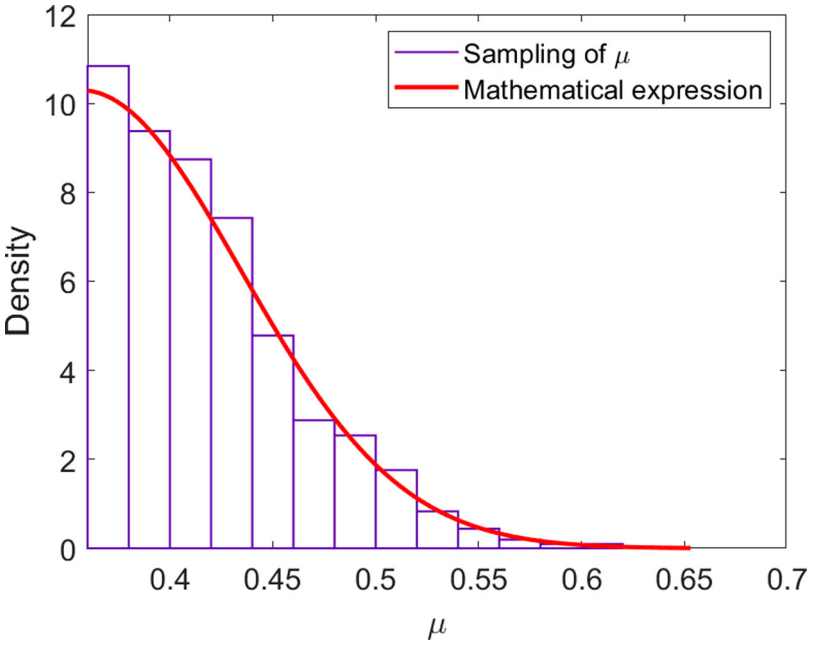

Figure 3. Probability density of the friction coefficient.

2.4. Probabilistic approach

Once the reduced model is built, its relevance is assessed by verifying its performance in a large number of random cases, in a Monte Carlo simulation. The purpose is to check that there is no evident difference in terms of variance between the direct simulation and the reduced model. The friction coefficient is chosen as the variable parameter in the Monte Carlo simulation, while the other two parameters are invariant. The vehicle speed is fixed at 80 km/h, and the axle load at 20 tons, corresponding to an experimental setup [26]. The friction coefficient is assumed to follow a one-sided normal distribution, representative of measured dry conditions, with a mean value of 0.36 and a standard deviation of 0.075 [27, 28]. The Monte Carlo solution includes 1024 samples, with the largest value being 0.62. In Figure 3 the bars are the probability density of the friction coefficient in the sampling group, while the red curve is the mathematical function. As a reference, 1024 full simulations are carried out using VOCO with the same sampling. For the dimension of the friction coefficient, the range of the Monte Carlo solution ([0.36, 0.62]) is included in the interval of the reduced model ([0.07, 0.7]). If the range needs to be larger, the previous model may be used with some additional calculations. The computing time and processing of the direct Monte Carlo simulation is about two days. These reference results are compared with the results of the s-PGD model.

3. Building of the reduced model by s-PGD approach

The s-PGD method has been used in this paper in order to build the reduced order model. The s-PGD approach is based on the same philosophy of separated representations as the PGD and enables the identification of complex physics existing in high dimensional

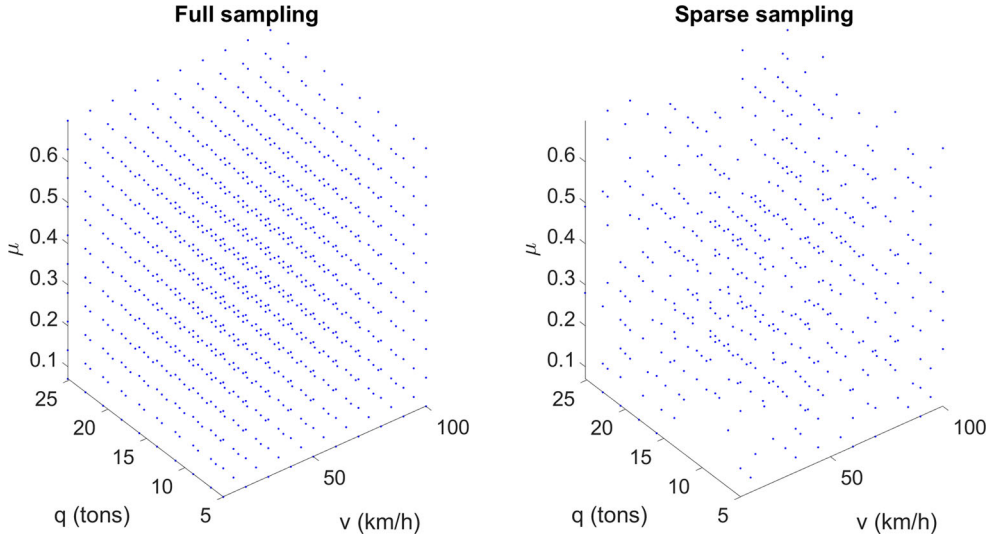

Figure 4. Sampling points in a three-dimensional space, adapted from [12]: full sampling of the speed, the axle load, and the friction coefficient (left), and sparse sampling (right).

settings from unstructured datasets. The data in these systems is often sparse due to the high dimensional nature of the phase space [13]. Mathematically, the tensors of spatial correlation function between the dimensions are sparse, as shown in Figure 4 for the three-dimensional space used in this study with variable vehicle speed, axle load and coefficient of friction. The s-PGD method does not require an *a priori* structure of the sampling points. The methods requiring such a regularity are usually anchored on Delaunay triangularization techniques, and use common interpolation techniques, i.e. linear, nearest, cubic, and natural [13].

The objective function $T_\gamma(v, q, \mu, x)$ lives in the Euclidean space $\mathbb{R}^4$, the goal of the s-PGD in the context of regression is to find an approximation ${T_\gamma}^M(v, q, \mu, x)$, which minimises the distance (usually related to the L2-norm):

$$ {T_\gamma}^M = \arg\min_{T_\gamma{}^*} \sum_{j=1}^{n_{sp}} T_\gamma\left(\overrightarrow{s_j}\right) - T_\gamma{}^*\left(\overrightarrow{s_j}\right)^2, \tag{3} $$

where $j = 1, \ldots, n_{sp}$ are the numbers of sampling points to train the model and $\overrightarrow{s_j} = (v_j, q_j, \mu_j, x_j)$ are the vectors which contain the data points of the training set. Supposing that there exists a ${T_\gamma}^M$, which satisfies the relation:

$$ T_\gamma\left(\overrightarrow{s_j}\right) - {T_\gamma}^M\overrightarrow{s_j} = 0, \tag{4} $$

the s-PGD approach begins by a Galerkin projection to convert Equation (4) into a weak form, the test function ${w_x}^*(v, q, \mu)$ is in the form as a set of Dirac delta functions collocated

at the sampling points:

$$w_x{}^*(v,q,\mu) = T_\gamma{}^*(v,q,\mu,x)\sum_{j=1}^{n_{sp}}\delta(\overrightarrow{s_j})$$
$$= (V_x^*(v)\cdot Q_x^M(q)\cdot U_x^M(\mu) + V_x^M(v)\cdot Q_x^*(q)\cdot U_x^M(\mu)$$
$$+ V_x^M(v)\cdot Q_x^M(q)\cdot U_x^*(\mu) + V_x^M(v)\cdot Q_x^M(q)\cdot U_x^M(\mu))\sum_{j=1}^{n_{sp}}\delta(\overrightarrow{s_j}), \quad (5)$$

which gives rise to

$$\int_\Omega w_x^*(v,q,\mu)\,(T_\gamma(v,q,\mu,x) - T_\gamma{}^M(v,q,\mu,x))\,dv\,dq\,du\,dx = 0, \quad (6)$$

where $\Omega = \mathbb{R}_v \times \mathbb{R}_q \times \mathbb{R}_\mu \times \mathbb{R}_x$ is the domain of interest.

In order to discretise Equation (6), each one-dimensional function of $T_\gamma{}^M$ is expressed by a polynomial in a matrix form:

$$V_x^i(v) = \sum_{k=0}^{N} N_k^i(v)\alpha_k^i = [N_0^i(v), N_1^i(v), \ldots, N_N^i(v)]\begin{vmatrix}\alpha_0^i\\ \alpha_1^i\\ \cdots\\ \alpha_N^i\end{vmatrix} = (\boldsymbol{N}_V^i(v))^T\boldsymbol{a}^i; \quad (7)$$

$$Q_x^i(q) = \sum_{k=0}^{N} N_k^i(q)\beta_k^i = [N_0^i(q), N_1^i(q), \ldots, N_N^i(q)]\begin{vmatrix}\beta_0^i\\ \beta_1^i\\ \cdots\\ \beta_N^i\end{vmatrix} = (\boldsymbol{N}_Q^i(q))^T\boldsymbol{b}^i; \quad (8)$$

$$U_x^i(\mu) = \sum_{k=0}^{N} N_k^i(\mu)\gamma_k{}^i = [N_0^i(\mu), N_1^i(\mu), \ldots, N_N^i(\mu)]\begin{vmatrix}\gamma_0^i\\ \gamma_1^i\\ \cdots\\ \gamma_N^i\end{vmatrix} = (\boldsymbol{N}_U^i(\mu))^T\boldsymbol{r}^i; \quad (9)$$

where $N_k^i(v)$, N_k^i(q) and $N_k^i(\mu)$ are the bases of interpolant polynomials; α_k^i, β_k^i and $\gamma_k{}^i$ are respectively their coefficients; k = 0, 1,… are respectively their coefficients: they represent the degrees of freedom of the chosen approximation. Low order (cubic N = 3) polynomials are adopted to avoid the Runge's phenomenon. The interested readers are invited to consult [13] for the technical details on how the equations like Equation (6) can be put in a matrix form. Using Equations (7)–(9) in Equation (6), we get a non-linear system:

$$\boldsymbol{M}_v\boldsymbol{a}^i = \boldsymbol{f}, \quad (10)$$

$$\boldsymbol{M}_q\boldsymbol{b}^i = \boldsymbol{f}, \quad (11)$$

$$\boldsymbol{M}_\mu\boldsymbol{r}^i = \boldsymbol{f}, \quad (12)$$

where:

$$\boldsymbol{f} = \begin{vmatrix}(T_\gamma(v_1,q_1,\mu_1,x_1) - T_\gamma{}^{M-1}(v_1,q_1,\mu_1,x_1)\\ \cdots\\ (T_\gamma(v_{n_{sp}},q_{n_{sp}},\mu_{n_{sp}},x_{n_{sp}}) - T_\gamma{}^{M-1}(v_{n_{sp}},q_{n_{sp}},\mu_{n_{sp}},x_{n_{sp}})\end{vmatrix},$$

$$\boldsymbol{M}_{\nu} = \begin{vmatrix} (\boldsymbol{N}_Q^i(q_1))^T \boldsymbol{b}^i (\boldsymbol{N}_U^i(\mu_1))^T \boldsymbol{r}^i (\boldsymbol{N}_V^i(\nu_1))^T \\ \cdots \\ (\boldsymbol{N}_Q^i(q_{n_{sp}}))^T \boldsymbol{b}^i (\boldsymbol{N}_U^i(\mu_{n_{sp}}))^T \boldsymbol{r}^i (\boldsymbol{N}_V^i(\nu_{n_{sp}}))^T \end{vmatrix},$$

$$\boldsymbol{M}_{q} = \begin{vmatrix} (\boldsymbol{N}_V^i(\nu_1))^T \boldsymbol{a}^i (\boldsymbol{N}_U^i(\mu_1))^T \boldsymbol{r}^i (\boldsymbol{N}_Q^i(q_1))^T \\ \cdots \\ (\boldsymbol{N}_V^i(\nu_{n_{sp}}))^T \boldsymbol{a}^i (\boldsymbol{N}_U^i(\mu_{n_{sp}}))^T \boldsymbol{r}^i (\boldsymbol{N}_Q^i(q_{n_{sp}}))^T \end{vmatrix},$$

$$\boldsymbol{M}_{\mu} = \begin{vmatrix} (\boldsymbol{N}_V^i(\nu_1))^T \boldsymbol{a}^i (\boldsymbol{N}_Q^i(q_1))^T \boldsymbol{b}^i (\boldsymbol{N}_U^i(\mu_1))^T \\ \cdots \\ (\boldsymbol{N}_V^i(\nu_{n_{sp}}))^T \boldsymbol{a}^i (\boldsymbol{N}_Q^i(q_{n_{sp}}))^T \boldsymbol{b}^i (\boldsymbol{N}_U^i(\mu_{n_{sp}}))^T \end{vmatrix},$$

The Equations (10)–(12) are solved by Ordinary Least Squares (OLS) supposing the other vectors are already known:

$$\boldsymbol{a}^i = (\boldsymbol{M}_{\boldsymbol{v}}^T \boldsymbol{M}_{\nu})^{-1} \boldsymbol{M}_{\boldsymbol{v}}^T \boldsymbol{f}, \tag{13}$$

$$\boldsymbol{b}^i = (\boldsymbol{M}_{\boldsymbol{q}}^T \boldsymbol{M}_{q})^{-1} \boldsymbol{M}_{\boldsymbol{q}}^T \boldsymbol{f}, \tag{14}$$

$$\boldsymbol{r}^i = (\boldsymbol{M}_{\mu}^T \boldsymbol{M}_{\mu})^{-1} \boldsymbol{M}_{\mu}^T \boldsymbol{f}, \tag{15}$$

The whole non-linear system can be solved by a non-linear solver (e.g. Picard or Newton) with a greedy algorithm. However, the sampling points (Figure 4, left) are separated randomly into two groups of parameters: the 'inside training' group (Figure 4, right), which gathers the points used to train the reduced model, and the 'outside training' group, used to validate the reduced model. This is done to avoid overfitting: if not, the reduced model would be tailored to a given dataset and cannot be generalised to other datasets.

4. Numerical results

4.1. Assessment of the s-PGD solution

The robustness of the s-PGD solution is assessed in this section. The relative residual related to the L2-norm between the reduced s-PGD model and the original data from the 'off-line' simulations, is in the form:

$$r_P{}^M = \frac{1}{n_{sp}} \sum_{j=1}^{n_{sp}} \sqrt{\frac{(T_\gamma(\nu_j, q_j, \mu_j, x_j) - T_\gamma{}^M(\nu_j, q_j, \mu_j, x_j))^2}{T_\gamma(\nu_j, q_j, \mu_j, x_j)^2}} \tag{16}$$

On the one hand, convergence is evaluated by checking if the variation of the residual between two iterations is smaller than a given tolerance. On the other hand, the 'outside training' residual should remain near the 'inside training' one. The relative residuals associated to the different sets 'inside the training', 'outside the training', and the complete set, are plotted in Figure 5. At the beginning of the iterative process, for instance with 5 modes, the difference between the relative residual of the inside and outside training may be important, showing that the number of modes is still too small. From 10 modes, the

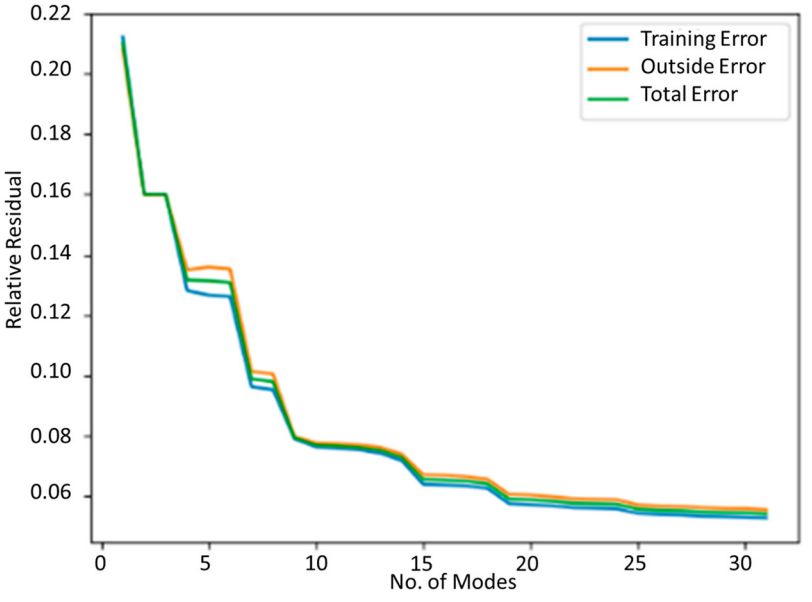

Figure 5. Convergence of the computational error. Relative residual r_P^N.

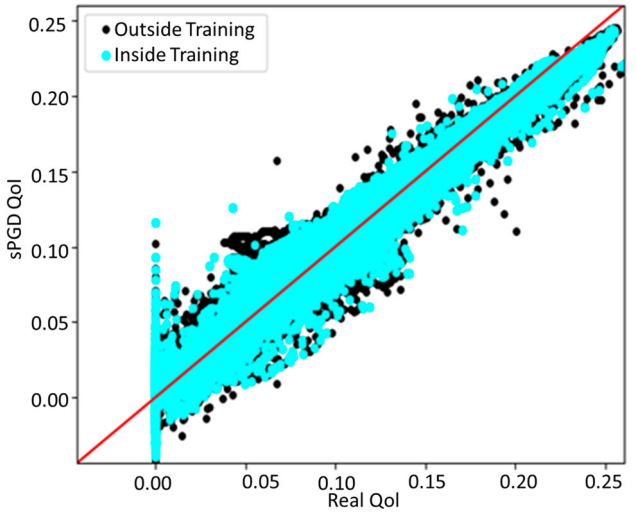

Figure 6. Point cloud of the full simulations versus s-PGD solution with 30 modes.

s-PGD solution is satisfactory for all points, but the relative residual is still too high. Both conditions of convergence are met with 30 modes.

From Figure 5, it can be seen that the enrichment process may be stopped after the 30th mode, as a fixed point has been reached. Moreover, Figure 6 gives a direct picture of the relation between the real simulations and the s-PGD solution with the results of 30 modes, where the QoI (quantity of interest) is, in the present case, T_γ. The abscissa is the value from the simulation, and the ordinate is the value from the s-PGD solution. The red line is the regression line whose slope is unity.

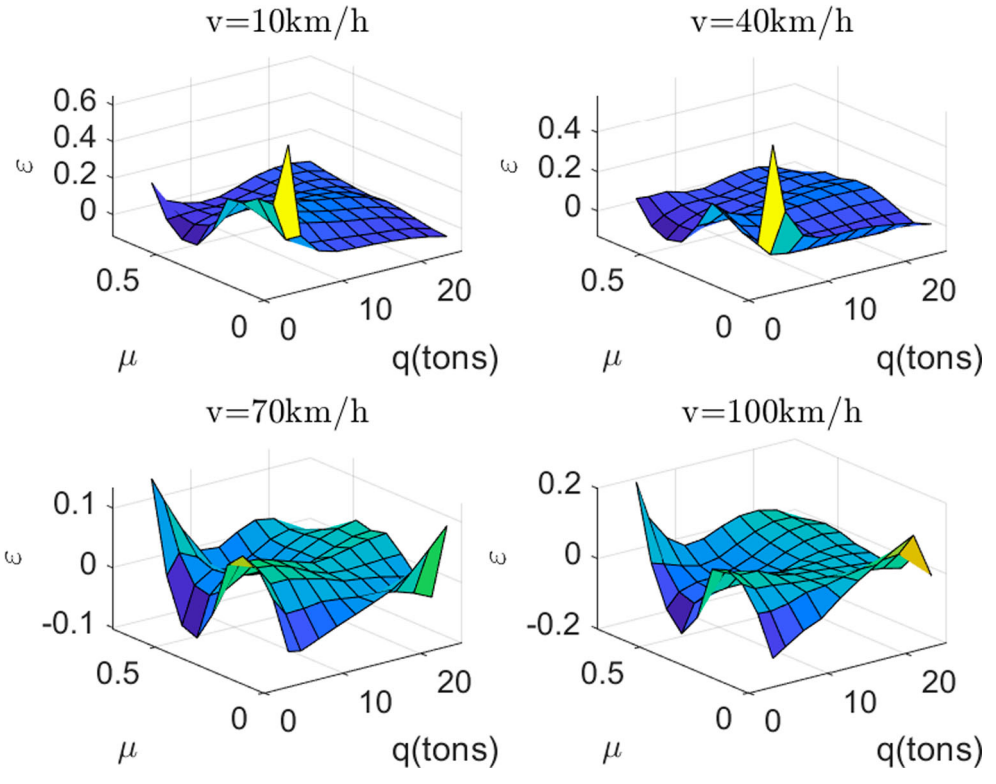

Figure 7. Relative difference ε of the T_γ peak.

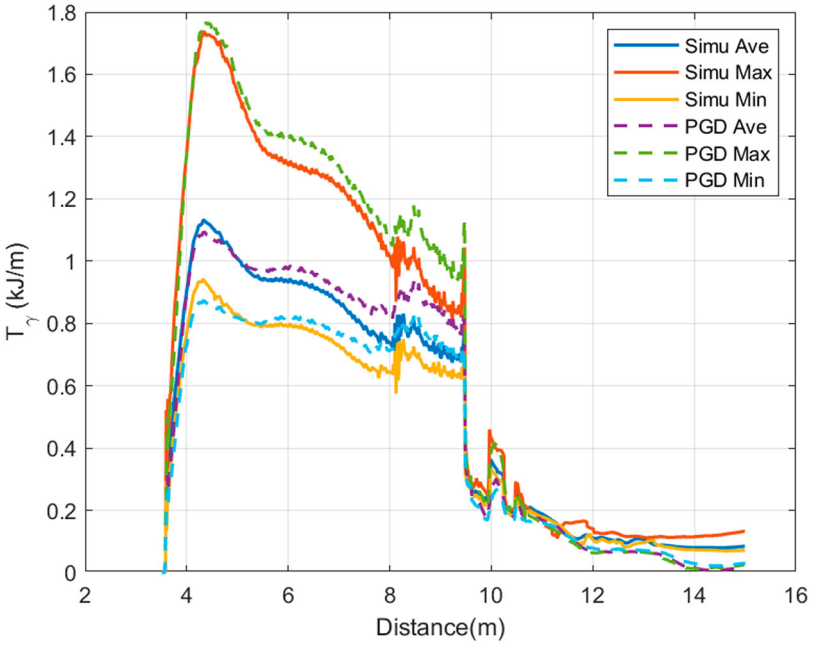

Figure 8. Extreme and average results of the T_γ function in spatial domain.

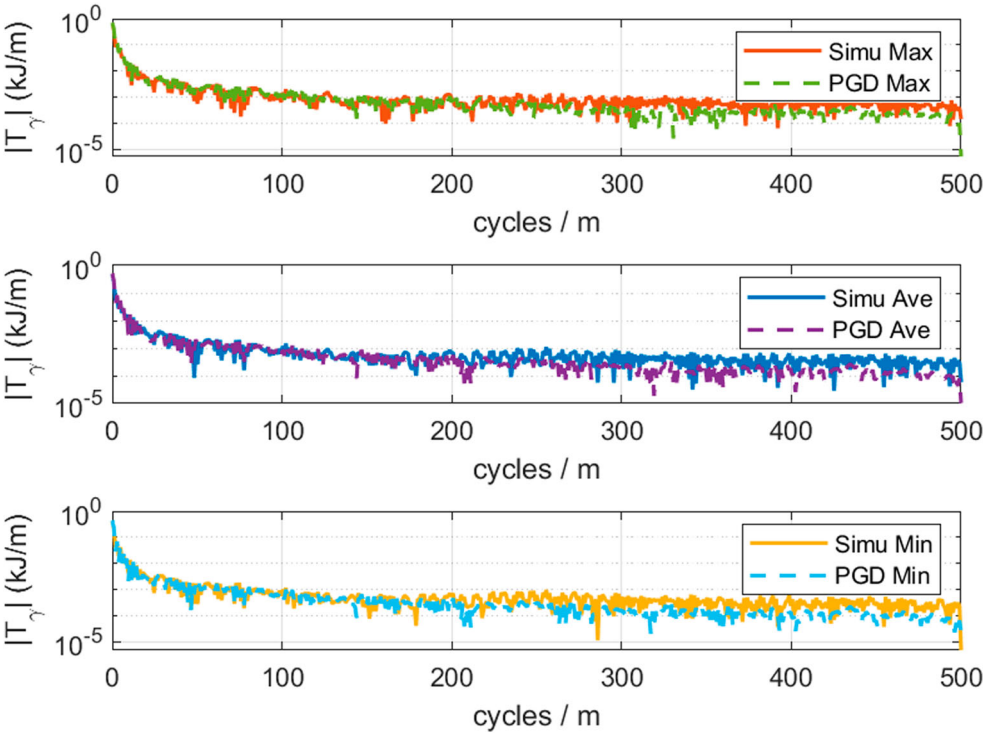

Figure 9. Fourier Transform of min, max and average results of the T_γ function in frequency domain for the direct and s-PGD simulations.

The peak of T_γ, located at the thinner part of the switch rail, can be chosen as a characteristic quantity to assess the PGD solution through the relative difference:

$$\varepsilon = \frac{\max_x T_\gamma{}^M(v,q,\mu,x) - \max_x T_\gamma(v,q,\mu,x)}{\max_x T_\gamma(v,q,\mu,x)} \tag{17}$$

Figure 7 shows the response surface of the relative difference between the results of the full simulation and the reduced s-PGD model with a constant speed, while the axle load and the friction coefficient vary. When the speed, the axle load and the friction coefficient are small, the relative error is large (top left and top right of Figure 7). When the speed is higher than 40 km/h, the relative error can be as high as 15% at the boundary of the parameter space (bottom left and bottom right of Figure 7). Using polynomial interpolation gives rise to Runge's phenomenon and getting precise results at the limit points of a given interval is not easy. Except at the boundaries of the domain, the absolute value of the relative error in the middle of the response surface is inferior to 5%, which is acceptable for the targeted engineering applications. In the following section, the reduced model is used as a numerical abacus in the context of probabilistic simulations.

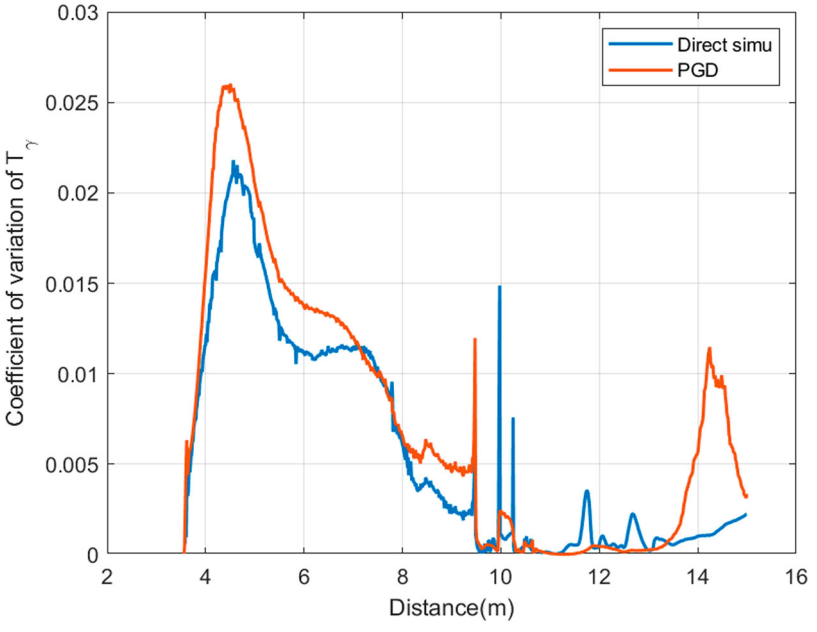

Figure 10. Coefficient of variance of the T_γ function.

4.2. Probabilistic simulation

This section presents the results of the probabilistic Monte Carlo simulation using 1024 samples of μ. Figure 8 presents the extreme and average results of the T_γ as a function of the distance in spatial domain with the results of 30 modes. The full lines are the results of the direct simulation; the dashed lines are the results of the reduced s-PGD model. It illustrates that the s-PGD solution is relevant with the simulation in the three cases. Figure 9 presents the Fourier transform with the results of 30 modes, where the results are satisfactory in the low-frequency domain (0 cycles/m – 200 cycles/m), while the high-frequency (200 cycles/m – 500 cycles/m) s-PGD values are smaller than those obtained using the direct simulation.

Figures 7 and 8 show the relevancy between the s-PGD solution and the simulation in the extreme cases and the mean value, but the comparison only involves a very small set of results. To discuss the accuracy of the approach in a more general way, Figure 10 presents the coefficients of variance of the T_γ to verify if they follow the same probability distribution. As can be seen, except for some peaks, there is no significant difference between the direct simulation and the reduced PGD model in statistical terms.

5. Conclusion

The PGD method is used in the context of railway dynamics for the first time in a non-intrusive way, at least to the knowledge of the authors. This is achieved through the use of the s-PGD approach which is a variant of the PGD method. One of the major advantages of the PGD method is to treat a multivariate problem as a series of one-dimensional sub-problems. Thus, the so-called curse of dimensionality is circumvented, enabling the

consideration of influence parameters usually not considered in design or maintenance. Furthermore, the resulting reduced model may be handled easily for subsequent tasks, such as design optimisation, inverse problems, or probabilistic studies.

A numerical abacus for evaluating the damage caused by the vehicles passing through S&C has been developed. A major hypothesis of the PGD method is the separability of the input parameters. In the studied case, the reduced order model is in good agreement with the full model. This seems to validate the applicability of the separated solution in the context of railway dynamics. As a verification of the method, a probabilistic study using the Monte Carlo method is subsequently carried out. The full model and the reduced one show comparable results, with a remarkable gain in terms of computation time. This is a significant advantage during the design phase of new railway network devices, when running full simulations with variable parameters can be significantly time consuming. The probabilistic study involves here a single parameter: the friction coefficient. Further studies should consider multivariate probabilistic analyse.

The use of the s-PGD method is non-intrusive, in the sense that no modification is needed in the source code of the MBS code VOCO. The only requirement is the availability of results to build the reduced order model. This non-intrusiveness opens up the possibility of using the PGD method with other MBS codes, thus broadening its application in the railway computational simulation domain.

In this first study, only three physical influence parameters are chosen. Other parameters such as the wheel and the rail profile, the track geometry or the class of rolling stock also play an important role in the durability of the turnout. Due to their complexity, taking into account these parameters is quite challenging. Considering these additional influence parameters to optimise the stiffness of the track components, such as the rail pads and the under-sleeper pads, should be addressed in future studies.

Acknowledgement

The authors wish to thank Rubén Ibáñez Pinillo, a post-doctoral researcher of the ESI Chair, ENSAM ParisTech, who has provided the s-PGD results. Without his generosity and contribution, this study could not have been achieved. The authors also want to acknowledge the fruitful discussions with Professor Francisco Chinesta.

Disclosure statement

No potential conflict of interest was reported by the author(s).

Funding

The authors would like to thank Association Nationale de la Recherche et de la Technologie (ANRT), and ESI Group for their financial support under the CIFRE [Grant No. 2017/1044].

ORCID

D. Fan http://orcid.org/0000-0002-3681-7325
A. Qazi http://orcid.org/0000-0002-4636-0103

References

[1] Wan C, Markine VL. Parametric study of wheel transitions at railway crossings. Veh Syst Dyn. 2015;53(12):1876–1901. doi:10.1080/00423114.2015.1089358.

[2] Pagaimo J, Magalhães H, Costa JN, et al. Derailment study of railway cargo vehicles using a response surface methodology. Veh Syst Dyn. 2020. doi:10.1080/00423114.2020.1815810.

[3] Kassa E, Nielsen JCO. Stochastic analysis of dynamic interaction between train and railway turnout. Veh Syst Dyn. 2008;46(5):429–449. doi:10.1080/00423110701452829.

[4] Burstow M. (2003). Whole Life Rail Model application and development: development of a rolling contact fatigue damage parameter. RSSB report.

[5] Pålsson BA. Design optimisation of switch rails in railway turnouts. Vehicle System Dynamics: International Journal of Vehicle Mechanics and Mobility. 2013;51(10):1619–1639.

[6] Chinesta F, Huerta A, Rozza G, et al. Encyclopedia of computational mechanics, chapter model order reduction. New York: John Wiley & Sons, Ltd; 2015.

[7] Kirchdoerfer T, Ortiz M. Data-driven computational mechanics. Computer Methods Applied Mechanics and Engineering. 2016;304:81–101.

[8] Kirchdoerfer T, Ortiz M. Data driven computing with noisy material data sets. Computer Methods AppliedMechanics and Engineering. 2017;326:622–641.

[9] Brunton SL, Proctor JL, Kutz JN. "Discovering governing equations from data by sparse identification of nonlinear dynamical systems," Proceedings of the National Academy of Sciences of the United States of America, vol. 113, no. 15, pp. 3932–3937, 2016.

[10] Quade M, Abel M, Kutz JN, et al. Sparse identification of nonlinear dynamics for rapid model recovery. Chaos: An Interdisciplinary Journal of Nonlinear Science. 2018;28(6):063116, 10 pages.

[11] Ly HV, Tran HT. Modeling and control of physical processes using proper orthogonal decomposition. Journal of Mathematical and Computer Modeling. 2001;33(1-3):223–236.

[12] Borzacchiello D, Aguado JV, Chinesta F. Non-intrusive sparse subspace learning for parametrized problems. Archives of Computational Methods in Engineering. 2019;26(2):303–326.

[13] Ibáñez R, Abisset-Chavanne E, Ammar A, et al. A multidimensional data-driven sparse identification technique: The sparse proper generalized decomposition. Complexity. 2018;2018:1–11.

[14] Ladevèze P. The large time increment method for the analysis of structures with non-linear behavior described by internal variables. Comptes Rendus de L'academie des Sciences Serie II. 1989;309(11):1095–1099.

[15] Polach O, Böttcher A, Vannucci D, et al. Validation of simulation models in the context of railway vehicle acceptance. Proceedings of the Institution of Mechanical engineers. Part F: Journal of Rail and Rapid Transit. 2015;229(6):729–754.

[16] Gregori S, Tur M, Nadal E, et al. Parametric model for the simulation of the railway catenary system static equilibrium problem. Finite Elem Anal Des. 2016;115:21–32.

[17] Gregori S, Tur M, Nadal E, et al. Fast simulation of the pantograph–catenary dynamic interaction. Finite Elem Anal Des. 2017;129:1–13.

[18] Kalker JJ. Book of tables for the Hertzian Creep-Force, in 2nd proceedings of the 2nd mini conf. on contact mechanics and wear of rail/wheel systems, Budapest (1996), p11.20.

[19] Chinesta F, Keunings R, Leygue A. The proper generalized decomposition for advanced numerical simulations. A primer. New-York: Springer Briefs in Applied Sciences and Technology; 2014.

[20] Chollet H, Sebès M, Maupu JL, et al. The VOCO multibody software in the context of real time simulation. Veh Syst Dyn; 2013;51(4):570–580.

[21] Bezin Y, Pålsson BA. Multibody simulation benchmark for dynamic vehicle-track interaction in switches and crossings: modelling description and simulation tasks. v3. University of Huddersfield, doi:10.34696/s60x-ay18 2019.

[22] Polach O, Bottcher A, Vannuci D, et al. Validation of multi-body models for simulation in authorisation of rail vehicles. 9th International Conference On Railway Bogies And Running Gears (Bogie 2013), Sep 2013, Budapest, Hungary. pp.187-196.

[23] Sebès M, Chollet H, Monteiro E, et al. (2015). Adaptation of the semi-Hertzian method to wheel/rail contact in turnouts. Proceedings of the 24th Symposium of the International Association for Vehicle System Dynamics (IAVSD 2015). Graz (Austria).
[24] Kassa E, Nielsen JCO. Dynamic interaction between train and railway turnout: full-scale field test and validation of simulation models. Vehicle System Dynamics: International Journal of Vehicle Mechanics and Mobility. 2008;46 sup1:521–534.
[25] Bezin Y, et al., Multibody simulation benchmark for dynamic vehicle-track interaction in switches and crossings: results and method statements. Submitted to VSD, 2021. doi:10.1080/00423114.2021.1942079.
[26] Pålsson BA, Nielsen JCO. Dynamic vehicle–track interaction in switches and crossings and the influence of rail pad stiffness –field measurements and validation of a simulation model. Veh Syst Dyn. 2015;53(6):734–755.
[27] European standard. (2018). EN 14363:2016+A1. Railway applications - testing and simulation for the acceptance of running characteristics of railway vehicles - Running Behaviour and stationary tests.
[28] Funfschilling C, Perrin G, Sebes M, et al. Probabilistic simulation for the certification of railway vehicles. Proceedings of the Institution of Mechanical Engineers, Part F: Journal of Rail and Rapid Transit. 2015;229(6):770–781.

Appendix

The goal of this section is to give a brief overview of the PGD method, without entering into technical details.

It is important to note that unlike classical model reduction approaches, PGD is an *a priori* approach, which does not rely on the availability of a complete solution to extract the reduced basis. It can rather be viewed as an efficient differential solver that builds the reduced basis progressively, depending on the desired accuracy of the solution.

The principle of the PGD approach can be illustrated by a parametric heat transfer equation with homogenous initial and boundary conditions [19]. For the sake of simplicity but without the loss of generality, the example lives in a one-dimensional space:

$$\frac{\partial u}{\partial t} - k\frac{\partial^2 u}{\partial x^2} - f = 0, \tag{A18}$$

where u is the temperature, f is the heat flow, x is the space coordinate, t is the time, and k is the conductivity considered as the additive parameter. The PGD method [15] employs the principle of separate representations to express $u(x, t, k)$ as a set of individual one-dimensional functions. This separated representation is constructed progressively. Thus, at each enrichment step M, the first $(M - 1)$ terms of the PGD approximation are already known:

$$u^{M-1}(x, t, k) = \sum_{i=1}^{M-1} X^i(x) \cdot T^i(t) \cdot K^i(k). \tag{A19}$$

To obtain the enriched PGD solution, the next term $X^M(x) \cdot T^M(t) \cdot K^M(k)$ can then be computed using a non-linear iterative scheme, which implies that iterations are needed at each enrichment step:

$$u^M(x, y) = u^{M-1}(x, t, k) \; + \; X^M(x) \cdot T^M(t) \cdot K^M(k). \tag{A20}$$

The computation of the M^{th} term is based on the weak form of the original equation using Galerkin projection schemes:

$$\int^{u^*} \left(\frac{\partial u}{\partial t} - k\frac{\partial^2 u}{\partial x^2} - f \right) dx\, dt\, dk = 0, \tag{A21}$$

where u^* is the separated form itself. Each of the three functions of the M^{th} mode is computed by assuming the remaining function pair to be already known. For the first iteration of all the modes,

the three functions are chosen randomly. By this operation, the original equation is transformed to an ordinary differential equation of the second order. The new equation can then be solved by standard mesh-based method such as finite difference method, finite element method etc. Thus, the complete problem is split into three one-dimensional sub-problems, enabling to circumvent the curse of dimensionality.

The final criterion of convergence is reached by comparing the last and the first mode with a given tolerance. Numerical experiments carried out so far with the PGD method show that the number of terms N required to obtain an accurate solution is not a function of the number of input parameters, but it rather depends on the separable nature of the exact solution [19].